PERGAMON

International Journal of Heat and Mass Transfer 42 (1999) 4321–4331

International Journal of HEAT and MASS TRANSFER

www.elsevier.com/locate/ijhmt

Fully developed forced convection through trapezoidal and hexagonal ducts

Rajashankar Sadasivam, Raj M. Manglik, Milind A. Jog*

Department of Mechanical, Industrial, and Nuclear Engineering, University of Cincinnati, Cincinnati, OH 45221-0072, USA

Received 4 January 1999; received in revised form 5 March 1999

Abstract

Laminar, fully developed flow through single- and double-trapezoidal (or hexagonal) ducts is modeled using a finite-difference method. A coordinate transformation is employed to map the irregular flow cross-section onto a rectangular computational domain. Both **H1** and **T** thermal boundary conditions are considered as they represent the fundamental limiting conditions in most practical applications. Solutions for velocity and temperature variations are obtained for a wide range of duct aspect ratios and with four different trapezoidal angles. The friction factor and Nusselt number results show a strong dependence on duct geometry (aspect ratio γ and trapezoidal angle θ). The variations of $f\,Re$, $Nu_{\mathbf{H1}}$, and $Nu_{\mathbf{T}}$ with duct aspect ratio for each θ-valued duct are presented in the form of polynomials in γ. These equations describe the computed numerical values within $\pm 2\%$ for single-trapezoidal and within $\pm 1.5\%$ for hexagonal ducts and are of much importance to the design of compact heat exchangers.

1. Introduction

The importance of analytical and experimental results for laminar forced convection in non-circular ducts to the practical design of a variety of compact heat exchangers cannot be overstated. In this study, hydrodynamically and thermally fully developed heat transfer in laminar flows of viscous liquids through single- and double-trapezoidal (hexagonal) ducts has been analyzed. These geometries represent flow channels of a variety of compact heat exchangers, as illustrated in Fig. 1. For example, the double-trapezoidal duct shape is encountered in lamella type compact heat exchangers, which find extensive usage in pulp and paper, alcohol, petrochemical and other chemical industries [1,2]. Likewise, the inter-plate flow channels in plate heat exchangers with washboard type corrugated plates are double trapezoidal. Plate heat exchangers are also used in a wide range of applications including food and chemical processing, refrigeration, and waste-heat recovery, among others [3]. The single-trapezoidal channel is employed in plate-fin heat exchangers [4], and micro-channel electronic cooling modules [5]. The hydraulic diameters of flow channels used in such heat exchangers are typically small and the length-to-diameter ratio (L/d_h) is relatively large. Due to these length scales and the viscous nature of the fluids being handled, the flow is usually laminar with fully developed conditions.

There has been considerable work on laminar forced-convective heat transfer in non-circular ducts reported in the literature. Shah and London [6], and Shah and Bhatti [7] give extended reviews of a large number of these studies. In some of the more recent literature, several different flow cross-section ge-

* Corresponding author. Tel.: +1-513-556-1675; fax: +1-513-556-3390.

E-mail address: milind.jog@uc.edu (M.A. Jog)

0017-9310/99/$ - see front matter
PII: S0017-9310(99)00091-5

Nomenclature

$b_0, \ldots, b_7$	constants in correlation for $f\,Re$ and Nu for flow in single-trapezoidal duct, Eq. (19)
$2b$	maximum width of the trapezoidal duct, Fig. 2, m
c	height of the trapezoidal duct, Fig. 2, m
$c_0, \ldots, c_7$	constants in correlation for $f\,Re$ and Nu for flow in double-trapezoidal duct, Eq. (20)
$2d$	width of the top wall of the trapezoidal duct, Fig. 2, m
d_h	hydraulic diameter, m
f	Fanning friction factor
h	dimensionless abscissa of the side-wall of the duct, Eq. (1)
h'	$(-1/\tan\theta)$
$\bar{h}(\bar{y})$	abscissa (distance from $\bar{y}=0$) of the side-wall of the trapezoidal duct, Fig. 2, m
H1	axially uniform wall heat flux with peripherally uniform wall temperature condition
H2	axially and peripherally uniform wall heat flux condition
k	thermal conductivity of fluid, W/(m K)
L	duct length, m
Nu	hydraulic-diameter based Nusselt number
p	pressure, Pa
Pe	Peclet number
Pr	Prandtl number
Re	hydraulic-diameter based Reynolds number
T	dimensionless temperature, Eq. (2)
$\bar{T}$	temperature, K
T_b	dimensionless mean or bulk fluid temperature
T	axially and peripherally uniform wall temperature condition
w	dimensionless axial flow velocity, Eq. (2)
$\bar{w}$	axial flow velocity, m/s
w_b	dimensionless mean or average axial flow velocity
x, y, z	dimensionless Cartesian coordinates, Eq. (1)
$\bar{x}, \bar{y}, \bar{z}$	Cartesian coordinates, m.

Greek symbols

α	thermal diffusivity, m^2/s
γ	aspect ratio of the trapezoidal duct, c/b or $c/2b$, Fig. 2
θ	included angle of trapezoidal duct cross-section, Figs. 1 and 2, degrees
μ	dynamic viscosity of the fluid, kg/(m s)
ξ, η	dimensionless transformed coordinates, Eq. (6)

ometries found in newer compact heat exchanger applications have been addressed [8,9]. These include double-sine [10], circular-segment [11], semi-circular [12,13], eccentric-annular [14], rhombic [15], regular polygonal [16], and several other unusual duct shapes [17]. To obtain theoretical solutions for laminar flow and heat transfer in such channels, different computational modeling techniques are usually employed and Sundén and Faghri [18], and Manglik and Bergles [9] have discussed the application of several such methodologies.

Fully developed laminar flow and heat transfer in a straight trapezoidal duct was first analyzed by Shah [19]. Employing a least-square boundary-value point-matching technique, series solutions for the velocity distribution, Fanning friction factor, temperature distribution and Nusselt number for the **H1** and **H2** boundary conditions are presented. Trapezoidal duct profiles described by $30^\circ \le \theta \le 75^\circ$ and $0 < \gamma < \infty$ have been considered. More recently, using a similar analytical technique, Flockart and Dhariwal [5] have reported pressure-drop results for fully developed laminar flows in a trapezoidal duct with $\theta = 54.74^\circ$. Farhanieh and Sundén [20] have reported graphical results for Nusselt number variation in the thermal entrance region of trapezoidal ducts with **T** boundary condition. These results clearly demonstrate the strong influence of the duct geometry on the thermal–hydraulic behavior. Asako et al. [21] have reported numerical solutions for periodically fully developed flow and heat transfer in a novel wavy (or zig-zag) channel with a trapezoidal cross section. In both the latter studies, finite-difference techniques were employed.

In this paper, thermally and hydrodynamically fully developed flow through both single- and double-trapezoidal (or hexagonal) ducts have been modeled using a finite-difference method. By using a coordinate transformation the irregular flow geometry is mapped into a rectangular computational domain. Solutions are obtained for a wide range of duct aspect ratios with four different trapezoid angles. Two thermal boundary conditions (**H1** and **T**), that are representative of the

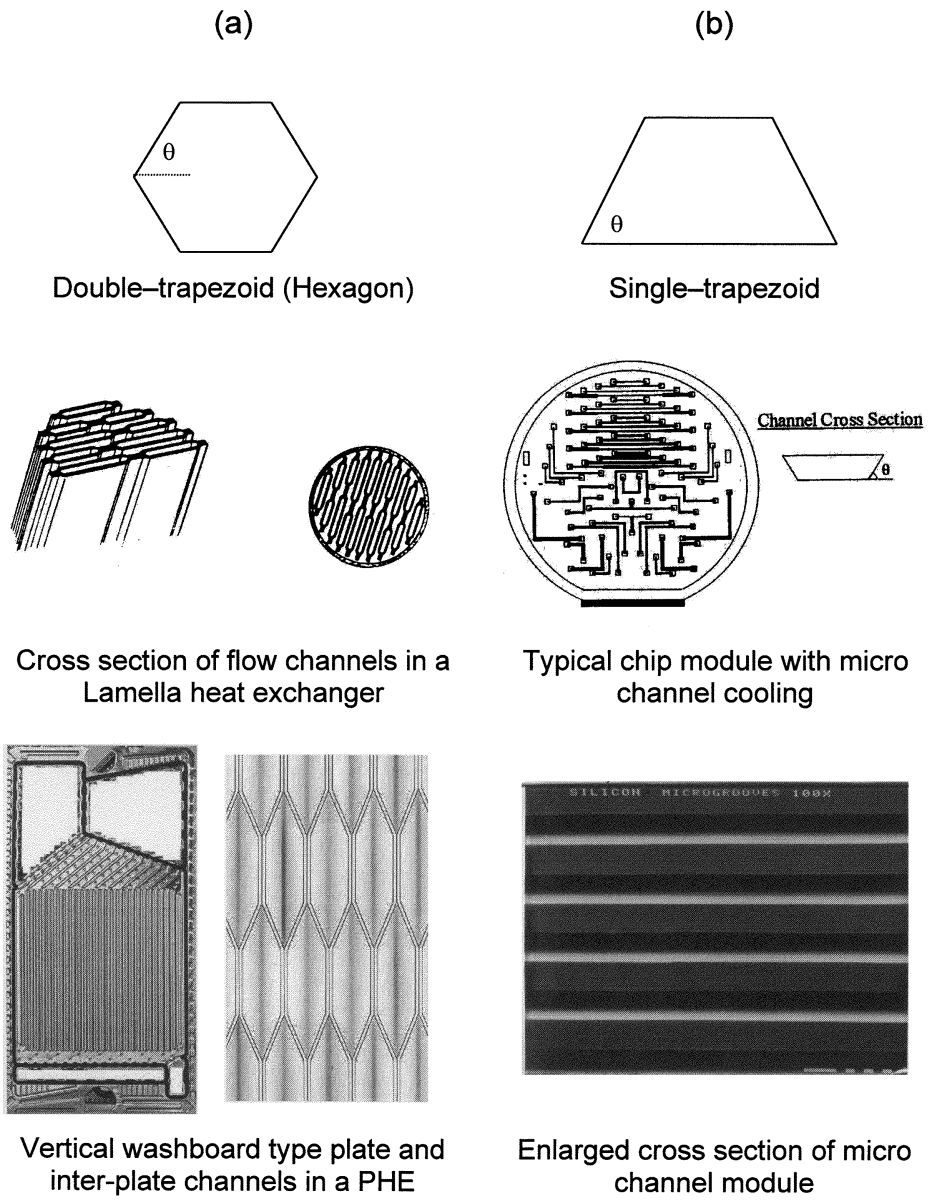

Fig. 1. Applications of trapezoidal and hexagonal shapes in heat exchange devices: (a) double-trapezoidal duct and (b) single-trapezoidal duct.

fundamental limiting conditions in most practical applications, have been considered. The **T** condition simulates, for example, heating of the process fluid stream by condensing steam; on the other hand, **H1** condition corresponds to heating or cooling in a two-fluid heat exchanger with equal capacity rates. Along with the velocity and temperature distributions, the friction factor and Nusselt number results for a wide range of trapezoidal and double-trapezoidal duct geometries are presented.

2. Mathematical formulation

The coordinate system, geometrical features, and the variables that describe the trapezoidal and double-trapezoidal (hexagonal) duct cross sections are shown in Fig. 2. Steady state, constant property, hydrodynamically and thermally fully developed laminar flows are considered. These conditions prevail for most viscous Newtonian liquid ($Pr \geq 1$) flows in long ducts of small hydraulic diameters ($L/d_h \gg 1$). Furthermore,

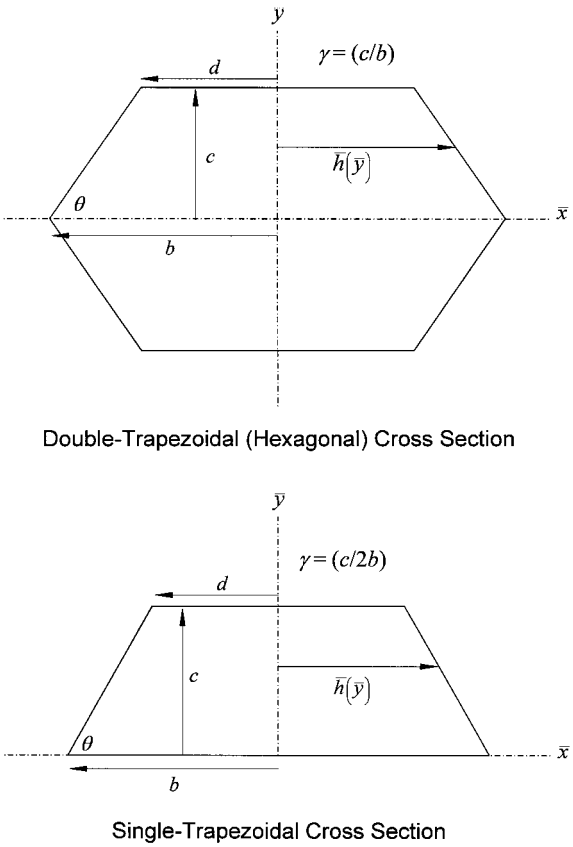

Fig. 2. Coordinate system and geometrical details of double- and single-trapezoidal duct cross sections.

axial conduction ($Pe \gg 1$) and viscous dissipation ($Br < 1$) are neglected. Thus, for such flow conditions, by introducing the following dimensionless forms of spatial variables, axial velocity, and temperature:

$$x = (\bar{x}/b), \quad y = (\bar{y}/b), \quad h = (\bar{h}/b) \tag{1}$$

$$w = \bar{w}/[(-\mathrm{d}p/\mathrm{d}\bar{z})(b^2/\mu)], \quad T = (\bar{T}_w - \bar{T})/[(b^2\bar{w}_b/\alpha)(\mathrm{d}\bar{T}_b/\mathrm{d}\bar{z})] \tag{2}$$

the momentum and energy conservation equations can be written as

$$\frac{\partial^2 w}{\partial x^2} + \frac{\partial^2 w}{\partial y^2} + 1 = 0 \tag{3}$$

$$\frac{\partial^2 T}{\partial x^2} + \frac{\partial^2 T}{\partial y^2} + S_T = 0 \tag{4}$$

where

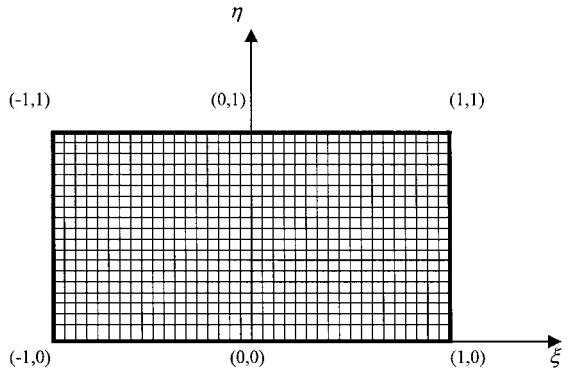

Fig. 3. A schematic representation of the computational domain.

$$S_T = \begin{cases} (w/w_b)(T/T_b) & \text{for } \mathbf{T} \text{ condition} \\ (w/w_b) & \text{for } \mathbf{H1} \text{ condition} \end{cases}$$

The governing equations are subject to no slip and uniform peripheral temperature conditions at the wall that are represented by the following:

Double-trapezoidal duct: $w = 0, \quad T = 0$ at

$$x = \pm 1, \quad y = \pm\gamma \tag{5a}$$

Trapezoidal duct: $w = 0, \quad T = 0$ at $x = \pm 1$,

$$y = \pm 2\gamma \tag{5b}$$

Furthermore, for double-trapezoidal ducts, in order to conserve computational time the symmetry about the x-axis is utilized and only half of the cross section is considered, for which

$$(\partial w/\partial y)_{y=0} = 0, \quad (\partial T/\partial y)_{y=0} = 0 \tag{5c}$$

To solve the governing equations using numerical methods, an appropriate grid needs to be developed to represent the flow cross section. It is clear from Fig. 2 that the sides of the duct do not conform to a rectilinear coordinate line, and using Cartesian coordinates will lead to half-grid cells and higher numerical errors. To overcome these difficulties, a grid that conforms to the boundaries of the duct is employed by effecting the following coordinate transformations:

$$\xi = [\bar{x}/\bar{h}(\bar{y})] = [x/h(y)], \quad \eta = (\bar{y}/c) = (yb/c), \quad h = [\bar{h}(\bar{y})/b] \tag{6}$$

This, in effect, maps the trapezoid/double-trapezoid shape into a unit rectangle, and a representation of the resulting computational grid is shown in Fig. 3. The governing equations in the transformed coordinates

can be expressed as

$$\left(\frac{1+\xi^2h'^2}{h^2}\right)\frac{\partial^2 w}{\partial\xi^2}+\left(\frac{b^2}{c^2}\right)\frac{\partial^2 w}{\partial\eta^2}+\left(\frac{2\xi h'^2}{h^2}\right)\frac{\partial w}{\partial\xi}-\left(\frac{2b\xi h'}{ch}\right)\frac{\partial^2 w}{\partial\xi\,\partial\eta}+1=0 \tag{7}$$

$$\left(\frac{1+\xi^2h'^2}{h^2}\right)\frac{\partial^2 T}{\partial\xi^2}+\left(\frac{b^2}{c^2}\right)\frac{\partial^2 T}{\partial\eta^2}+\left(\frac{2\xi h'^2}{h^2}\right)\frac{\partial T}{\partial\xi}-\left(\frac{2b\xi h'}{ch}\right)\frac{\partial^2 T}{\partial\xi\,\partial\eta}+S_{\mathrm{T}}=0 \tag{8}$$

Here $h'=(\mathrm{d}h/\mathrm{d}y)=-(1/\tan\theta)$, and the boundary conditions can be restated as

Double-trapezoidal duct:

$$w(-1,\eta)=w(1,\eta)=w(\xi,1)=0,$$

$$T(-1,\eta)=T(1,\eta)=T(\xi,1)=0 \tag{9a}$$

Single-trapezoidal duct (in addition to Eq. (9a)):

$$w(\xi,0)=0,\quad T(\xi,0)=0 \tag{9b}$$

The symmetry condition of Eq. (5c) for the double-trapezoidal duct is given by

$$\left[\left(\frac{b}{c}\right)\frac{\partial w}{\partial\eta}-\left(\frac{\xi h'}{h}\right)\frac{\partial w}{\partial\xi}\right]_{(\xi,0)}=0,$$

$$\left[\left(\frac{b}{c}\right)\frac{\partial T}{\partial\eta}-\left(\frac{\xi h'}{h}\right)\frac{\partial T}{\partial\xi}\right]_{(\xi,0)}=0 \tag{9c}$$

In order to determine the average frictional loss and heat transfer coefficient from the velocity and the temperature distributions, the dimensionless bulk velocity and temperature are calculated from their usual definitions as

Double-trapezoidal duct:

$$w_{\mathrm{b}}=\frac{1}{[2-(\gamma\ \tan\ \theta)]}\int_{\xi=-1}^{\xi=1}\int_{\eta=0}^{\eta=1} wh\,\mathrm{d}\eta\,\mathrm{d}\xi \tag{10}$$

$$T_{\mathrm{b}}=\frac{1}{[2-(\gamma\ \tan\ \theta)]}\int_{\xi=-1}^{\xi=1}\int_{\eta=0}^{\eta=1} wh\,\mathrm{d}\eta\,\mathrm{d}\xi \tag{11}$$

Single-trapezoidal duct:

$$w_{\mathrm{b}}=\frac{1}{[2-(2\gamma\ \tan\ \theta)]}\int_{\xi=-1}^{\xi=1}\int_{\eta=0}^{\eta=1} wh\,\mathrm{d}\eta\,\mathrm{d}\xi \tag{12}$$

$$T_{\mathrm{b}}=\frac{1}{[2-(2\gamma\ \tan\ \theta)]}\int_{\xi=-1}^{\xi=1}\int_{\eta=0}^{\eta=1} Th\,\mathrm{d}\eta\,\mathrm{d}\xi \tag{13}$$

Finally, the hydraulic-diameter based Fanning friction factor is given by

$$f\,Re=(d_{\mathrm{h}}/b)^2(1/2w_{\mathrm{b}}) \tag{14}$$

and the fully-developed flow Nusselt number, for both **H1** and **T** conditions, is given by

$$Nu=(d_{\mathrm{h}}/b)^2(1/4T_{\mathrm{b}}) \tag{15}$$

The hydraulic diameters for the two ducts are calculated as

$$d_{\mathrm{h}}=\begin{cases}\dfrac{2c[2-(\gamma/\tan\ \theta)]}{1-(\gamma/\sin\ \theta)(\cos\ \theta-1)} & \text{(double-trapezoidal duct)}\\[2ex] \dfrac{2c[2-(\gamma/\tan\ \theta)]}{2-(\gamma/\sin\ \theta)(\cos\ \theta-1)} & \text{(trapezoidal duct)}\end{cases} \tag{16}$$

3. Computational methodology

The transformed governing partial differential equations are discretized and solved using finite-difference techniques. For all duct cross-section geometries considered in this study, the computational domain in $(\xi,\ \eta)$ was described by a uniform grid. Second-order accurate, central differencing was employed for the discretized representation of Eqs. (7) and (8). Straightforward Dirichlet boundary conditions ($w=0$ and $T=0$) are applied at the walls; in the case of double-trapezoidal ducts, however, second-order backward differencing was used at the $\eta=0$ ($y=0$) mid plane to represent the Neumann or symmetry boundary condition. Furthermore, Simpson's rule was employed to carry out the numerical integration for calculating the bulk velocity and temperature.

All computations were performed using a uniform 121×61 ($\xi\times\eta$) grid, with the discretized equations solved by the point-iterative Gauss–Siedel method. The iterations were performed over the computational domain bounded by $\eta=0$ to $\eta=1$. The convergence criterion (maximum relative error in values of the dependent variable between two successive iterations) was set to 10^{-6} in all cases. To test grid independence of the computational solutions, the use of a 161×81 grid produced no change in the calculated values of $f\,Re$ and Nu (**T** and **H1**) in a regular hexagon duct ($\theta=60^\circ$ and $\gamma=0.867$).

The numerical accuracy of the computations was primarily verified by comparing the $f\,Re$ and Nu (**T**

and **H1**) values calculated from Eqs. (14) and (15), respectively, with those obtained from the peripherally averaged wall gradients given by

$$f\,Re = -\frac{2d_h}{w_b}\int_{wall}\left.\frac{\partial w}{\partial n}\right|_{wall} ds \tag{17}$$

$$Nu = -\frac{d_h}{T_b}\int_{wall}\left.\frac{\partial T}{\partial n}\right|_{wall} ds \tag{18}$$

where n denotes the normal direction to the duct wall and s is the distance along the duct wall. The differences between the two sets of values obtained from Eqs. (14), (15), (17) and (18) were generally less than 2%, with a maximum deviation of 4% in the results for the duct with $\gamma = 0.01$. Additionally, as presented in the next section, $f\,Re$ and $Nu_{\mathbf{H1}}$ results for single-trapezoidal ducts are in excellent agreement with those reported by Shah [19].

4. Results and discussion

Numerical solutions for fully developed laminar flow and heat transfer in a wide range of trapezoidal and double-trapezoidal (hexagonal) duct geometries, that represent flow cross sections in many different compact heat exchange devices, are presented in the ensuing sections. The flow and temperature distributions, along with the friction factor and Nusselt numbers results, highlight the influence of the duct geometry (θ and γ) and wall heating/cooling conditions on the thermal–hydraulic performance and provide useful design data.

4.1. Trapezoidal ducts

The isothermal friction factor ($f\,Re$) and Nusselt number ($Nu_{\mathbf{H1}}$ and $Nu_{\mathbf{T}}$) results for trapezoidal ducts described by $\theta = 30$, 45, 60, and 75°, and varying aspect ratios ($\gamma = c/2b$; see Fig. 2) are presented in Figs. 4–6, respectively. Here, the results for $f\,Re$ and $Nu_{\mathbf{H1}}$ also serve to verify the accuracy of numerical solutions. This is seen in Figs. 4 and 5, where they are compared with the analytical solutions reported by Shah [19]. The excellent agreement between the two is clearly evident, and this amply validates the computational methodology, grid selection, and the precision of the numerical values.

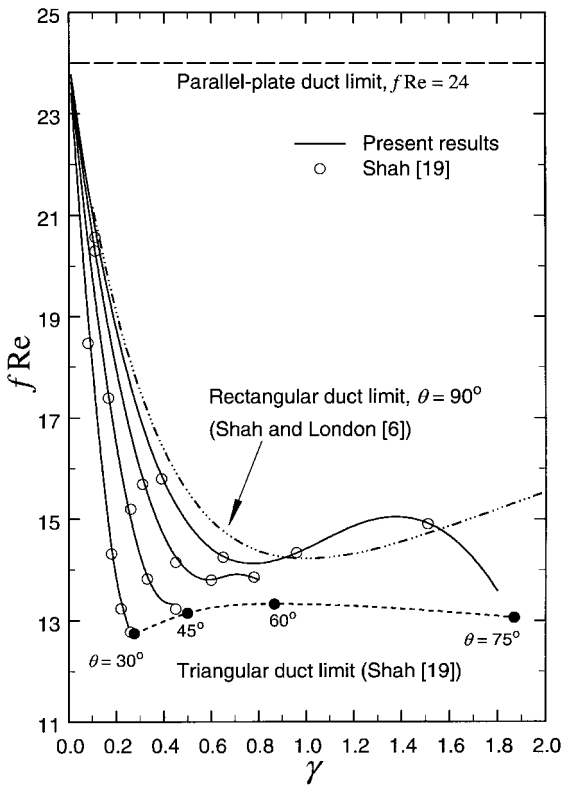

Fig. 4. Variation of $f\,Re$ with aspect ratio γ of a trapezoidal duct.

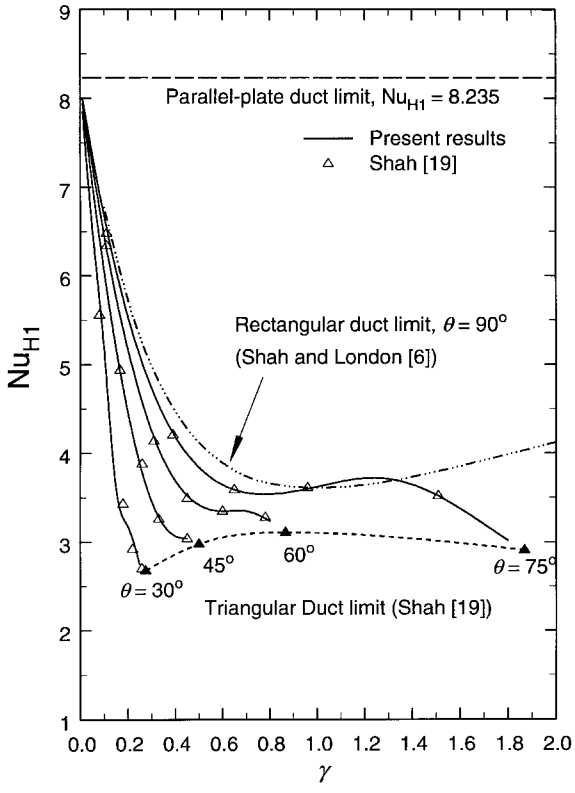

Fig. 5. Variation of $Nu_{\mathbf{H1}}$ with aspect ratio γ of a trapezoidal duct.

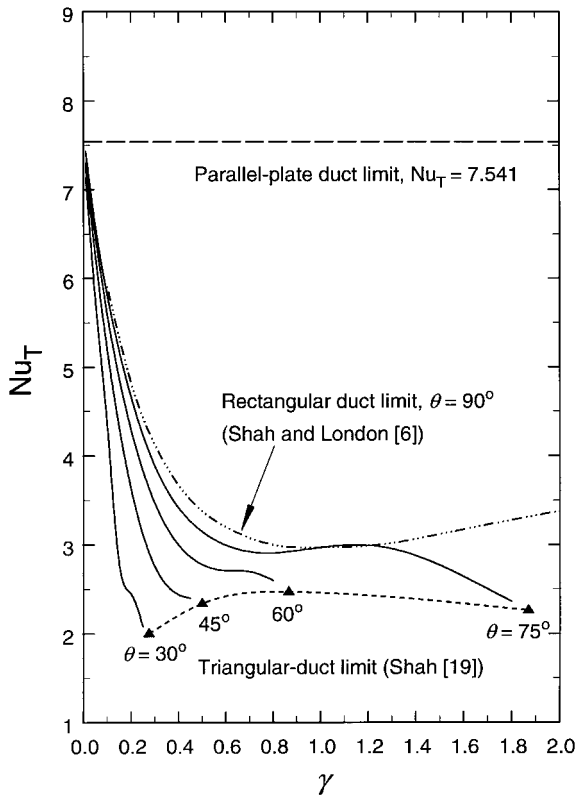

Fig. 6. Variation of $Nu_{\mathbf{T}}$ with aspect ratio γ of a trapezoidal duct.

Figs. 4–6 clearly illustrate the influence of the trapezoidal ducts' geometrical features (described by θ and γ) on the fully developed laminar flow $f\,Re$, $Nu_{\mathbf{H1}}$ and $Nu_{\mathbf{T}}$, respectively. For the variation with γ, the maximum aspect ratio for a given θ-valued trapezoidal duct is defined by the respective triangular duct limit. The lower aspect ratio limit, is represented by the parallel-plate duct when $\theta \to 0$ or $\gamma \to 0$ ($f\,Re = 24$, $Nu_{\mathbf{H1}} = 8.235$ and $Nu_{\mathbf{T}} = 7.541$). For $0^\circ < \theta < 60^\circ$, in Fig. 4, ($f\,Re$) is seen to monotonically decrease with increasing γ to the triangular duct limit. For $60^\circ \leq \theta \leq 90^\circ$, however, $f\,Re$ is first seen to decrease, then increase before again decreasing to the triangular duct limit with increasing γ. The upper θ-limit of the duct geometry is described by $\theta = 90^\circ$, or a rectangular duct, and the $f\,Re$ results given by Shah and London [6] are also graphed in Fig. 4. These, of course, are symmetric about $\gamma = 1$ (square duct). Similar behaviors in the variation of $Nu_{\mathbf{H1}}$ and $Nu_{\mathbf{T}}$ with θ and γ are seen in Figs. 5 and 6, respectively.

The variation of $f\,Re$ as well as Nu (for both **T** and **H1** boundary conditions) with aspect ratio for each θ-valued trapezoidal duct can be represented by the following polynomial in γ:

$f\,Re$ or

$$Nu = b_0 + b_1\gamma + b_2\gamma^2 + b_3\gamma^3 + b_4\gamma^4 + b_5\gamma^5 + b_6\gamma^6 + b_7\gamma^7 \quad (19)$$

The values of the constants b_0–b_7 are given in Table 1 for $\theta = 30$, 45, 60 and 75° trapezoidal cross sections. Eq. (19) describes the computed numerical values within ±2% in all cases.

4.2. Double-trapezoidal ducts

In double-trapezoidal (or hexagonal) ducts, the laminar fully developed velocity field is strongly influenced by the aspect ratio of the flow cross section. This is seen in Fig. 7, where the velocity profiles for three different aspect ratios ($\gamma = 0.5$, 1.5 and 2.5) of the duct with included angle $\theta = 75^\circ$ are presented. Note that the duct geometry is symmetric about x- and y-axes, and hence only a quadrant of the flow cross section is shown. The results indicate a rather complex interaction between the duct geometry and the developed flow field. As the aspect ratio increases ($\gamma > 0$), the flow gets 'squeezed' into the core region by sharp corners of the boundaries and the peak velocity increases. The flow distribution (that is more 'uniform' with large wall gradients in small γ ducts) gets more 'conical'

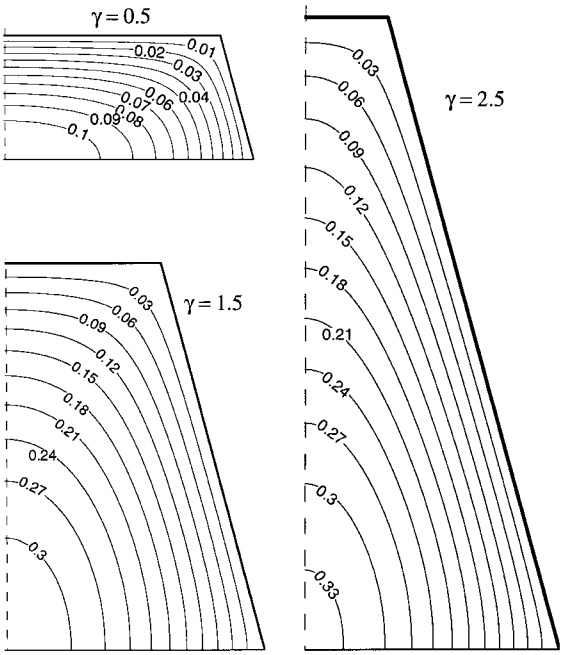

Fig. 7. Dimensionless isovelocity profiles for fully developed laminar flow through double-trapezoidal ducts of three different aspect ratios and included angle $\theta = 75^\circ$.

Table 1
Values of constants b_0–b_7 in Eq. (19) for single trapezoidal ducts with four different θ angles

	$\theta=30^\circ$			$\theta=45^\circ$			$\theta=60^\circ$			$\theta=75^\circ$		
	$f\,Re$	$Nu_{\mathbf{H1}}$	$Nu_{\mathbf{T}}$	$f\,Re$	$Nu_{\mathbf{H1}}$	$Nu_{\mathbf{T}}$	$f\,Re$	$Nu_{\mathbf{H1}}$	$Nu_{\mathbf{T}}$	$f\,Re$	$Nu_{\mathbf{H1}}$	$Nu_{\mathbf{T}}$
b_0	24.000	8.2350	7.5410	24.000	8.2350	7.5410	24.000	8.2350	7.5410	24.000	8.2350	7.5410
b_1	−66.335	−36.138	−39.551	−40.015	−28.188	−29.251	−38.909	−20.951	−23.175	−33.658	−17.642	−20.183
b_2	14.580	107.54	155.04	−127.22	134.47	90.601	48.056	39.219	40.937	39.320	24.711	33.483
b_3	540.43	−1196.2	−1699.6	1448.3	−1206.2	−535.56	−44.278	−82.077	−34.727	−18.584	−16.852	−26.286
b_4	−1618.9	6468.3	9621.5	−5523.3	6854.2	2824.4	72.094	172.33	18.793	3.7740	7.0934	9.9036
b_5	2478.5	−7824.5	−16592	10081	−20679	−8045.9	−51.027	−183.90	7.6346	−0.45060	−2.2892	−1.4825
b_6	0.000	−8280.3	0.000	−7035.6	31782	11583	0.000	70.105	0.000	0.000	0.39886	0.000
b_7	0.000	0.000	0.000	0.000	−19592	−6702.8	0.000	0.000	0.000	0.000	0.000	0.000

with smaller velocity gradients at the wall. Furthermore, for $\theta=75^\circ$ double-trapezoidal ducts, the peak core velocity increases sharply as γ increases from 0 to about 1.0, and then attains a plateau as $\gamma \to 2.5$; for higher γ, $w_{\max}$ decreases slightly. This change in magnitude of $w_{\max}$ can be ascertained from Table 2.

The influence of duct geometry and flow distribution on the temperature field is depicted in Fig. 8 for **H1** boundary condition, and in Fig. 9 for the **T** boundary condition. In both these figures, isotherms in $\theta=75^\circ$ double-trapezoidal ducts with $\gamma=0.5$, 1.5 and 2.5 are presented. Once again, reflecting the convective effects of the flow field, the maximum core temperature increases with increasing γ, and representative values for both **H1** and **T** conditions are listed in Table 2. The temperature field correspondingly tends to be more conical in profile, with smaller wall gradients. However, the wall gradients are relatively sharper with the **H1** condition in comparison with the **T** boundary condition.

Given the velocity and temperature fields, the variations with θ and γ in the concomitant fully developed isothermal Fanning friction factors and Nusselt numbers are presented in Figs. 10–12. For each θ-valued double-trapezoidal duct, the limiting conditions for the variation with aspect ratio are described by the results for the parallel plate channel ($\gamma \to 0$) and those for rhombic ducts ($\gamma \to \gamma_{\max}$). The $f\,Re$ and $Nu_{\mathbf{H1}}$ results for rhombic ducts have been previously reported by Shah [19], and $Nu_{\mathbf{T}}$ results by Asako and Faghri [15].

Displaying a performance somewhat similar to trapezoidal ducts, the impact of the double-trapezoidal (or hexagonal) flow cross-section geometry variations on $f\,Re$, $Nu_{\mathbf{H1}}$ and $Nu_{\mathbf{T}}$ is depicted in Figs. 10–12, respectively. For $\theta < 45^\circ$ ducts, in Fig. 10 for example, f

Table 2
Maximum values of dimensionless velocities and temperatures for fully developed laminar flow in double-trapezoidal duct of included angle $\theta=75^\circ$ and different aspect ratios γ

γ	$w_{\max}$	$T_{\max}$ (**H1**)	$T_{\max}$ (**T**)
0.1	4.91E−03	6.42E−03	0.0112
0.5	0.1102	0.1667	0.2312
1.0	0.2623	0.3964	0.5218
1.5	0.3236	0.4918	0.6665
2.0	0.3377	0.5266	0.7575
2.5	0.3392	0.5531	0.8374
3.0	0.3387	0.5778	0.8932
3.5	0.3379	0.5935	0.9459

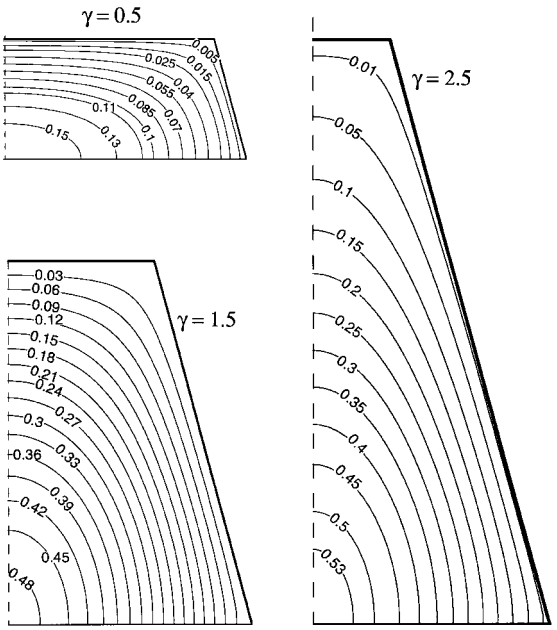

Fig. 8. Dimensionless temperature distribution in fully developed laminar flow in double-trapezoidal duct of three different aspect ratios and included angle $\theta=75^\circ$ (**H1** boundary condition).

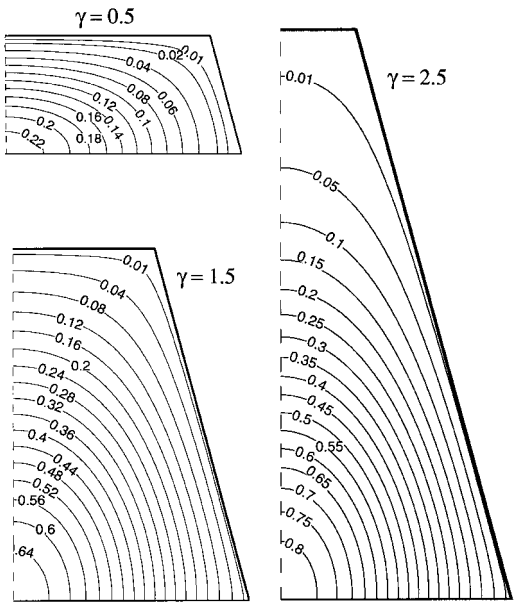

Fig. 9. Dimensionless temperature distribution in fully developed laminar flow in double-trapezoidal duct of three different aspect ratios and included angle $\theta = 75^\circ$ (**T** boundary condition).

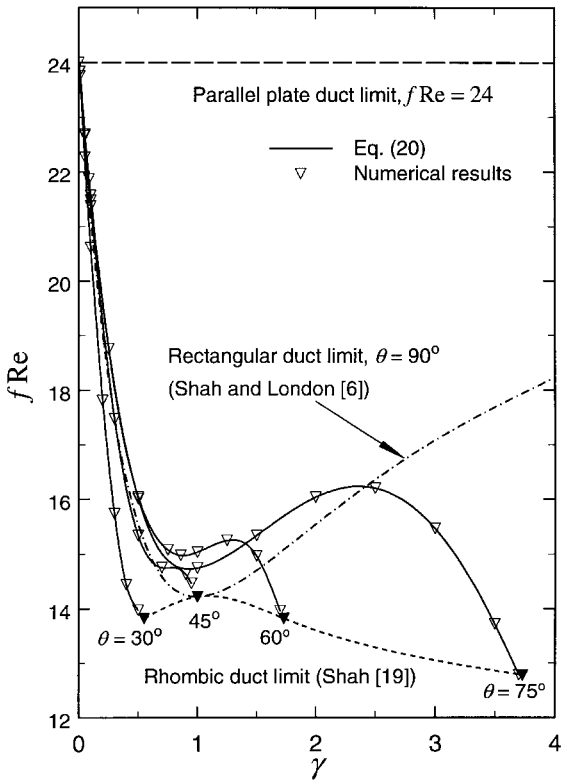

Fig. 10. Variation of $f\ Re$ with aspect ratio γ of a double-trapezoidal (hexagonal) duct.

Re is seen to decrease monotonically with increasing γ up to the limit represented by a rhombic duct. With $\theta \geq 45^\circ$, on the other hand, $f\ Re$ first decreases, and then increases to a higher 'plateau' value before finally decreasing to the rhombic-duct limit. This behavior is most pronounced in the $\theta = 75^\circ$ double-trapezoid ducts. Besides the parallel-plate and rhombic duct limits, the results for rectangular ducts define the $\theta = 90^\circ$ limit. These results are, of course, symmetric about $\gamma = 1$ (square duct with $\theta = 90^\circ$ or rhombic duct with $\theta = 45^\circ$). Figs. 11 and 12, respectively, show qualitatively similar $Nu_{\mathbf{H1}}$ and $Nu_{\mathbf{T}}$ performances. Also, as would be expected with the uniform heat flux boundary condition (**H1**) and the consequent steeper wall temperature gradients, $Nu_{\mathbf{H1}} > Nu_{\mathbf{T}}$ for all cases.

Finally, the computed results for $f\ Re$, $Nu_{\mathbf{H1}}$, and $Nu_{\mathbf{T}}$ in double-trapezoidal (hexagonal) ducts can be correlated by the following polynomial in γ for each θ-case:

Table 3
Values of constants c_0–c_8 in Eq. (20) for double-trapezoidal ducts with four different θ angles

	$\theta = 30^\circ$			$\theta = 45^\circ$			$\theta = 60^\circ$			$\theta = 75^\circ$		
	$f\ Re$	$Nu_{\mathbf{H1}}$	$Nu_{\mathbf{T}}$	$f\ Re$	$Nu_{\mathbf{H1}}$	$Nu_{\mathbf{T}}$	$f\ Re$	$Nu_{\mathbf{H1}}$	$Nu_{\mathbf{T}}$	$f\ Re$	$Nu_{\mathbf{H1}}$	$Nu_{\mathbf{T}}$
c_0	24.000	8.2350	7.5410	24.000	8.2350	7.5410	24.000	8.2350	7.5410	24.000	8.2350	7.5410
c_1	−35.572	−10.718	−15.619	−25.420	−8.073	−13.089	−25.845	−10.143	−11.131	−26.880	−12.927	−14.012
c_2	−0.6031	−118.93	−46.383	−47.905	−76.284	−16.657	13.240	−19.369	−28.576	27.464	13.714	14.695
c_3	171.31	939.99	339.03	473.67	479.40	135.66	42.287	126.62	196.47	−12.308	−6.3841	−1.9451
c_4	−352.65	−3139.4	−682.51	−1443.4	−1269.5	−251.14	−90.073	−262.88	−434.82	2.5841	1.3521	−7.0212
c_5	271.91	5031.3	480.87	2223.1	1767.7	204.26	81.018	295.86	507.47	−0.21431	−0.10905	5.7802
c_6	0.000	−3079.8	0.000	−1687.9	−1247.6	−63.553	−35.797	−190.22	−331.80	0.000	0.000	−2.0413
c_7	0.000	0.000	0.000	498.34	0.000	0.000	6.1894	65.246	114.53	0.000	0.000	0.35003
c_8	0.000	0.000	0.000	0.000	0.000	0.000	0.000	−9.2412	−16.238	0.000	0.000	−0.02401

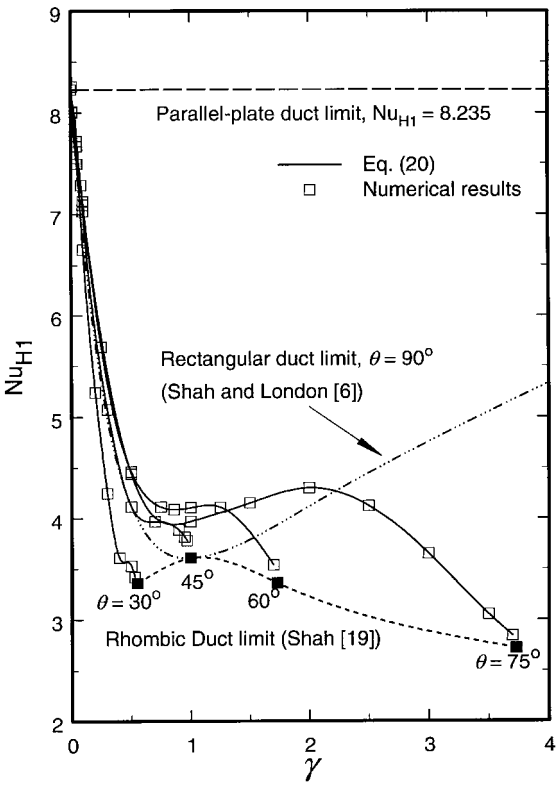

Fig. 11. Variation of Nu_{H1} with aspect ratio γ of a double-trapezoidal (hexagonal) duct.

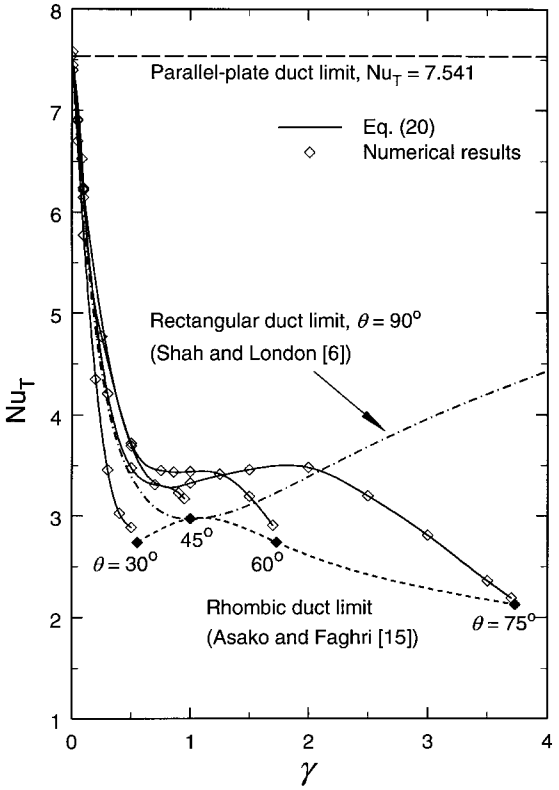

Fig. 12. Variation of Nu_T with aspect ratio γ of a double-trapezoidal (hexagonal) duct.

$f\,Re$ or

$$Nu = c_0 + c_1\gamma + c_2\gamma^2 + c_3\gamma^3 + c_4\gamma^4 + c_5\gamma^5 + c_6\gamma^6 + c_7\gamma^7 + c_8\gamma^8 \quad (20)$$

The values of the constants, c_0–c_8, for each set of geometries described by $\theta = 30$, 45, 60 and 75° are listed in Table 3. This equation describes the numerical results for each θ case and their variation with γ to within $\pm 1.5\%$.

Acknowledgement

This study was supported in part by the National Science Foundation under Grant nos CTS-9502128 (R.M.M.) and CTS-9733369 (M.A.J.).

References

[1] E.A.D. Saunders, Heat Exchangers: Selection, Design and Construction, Longman, Harlow, UK, 1998.
[2] G. Walker, Industrial Heat Exchangers, Hemisphere, New York, 1990.
[3] R.M. Manglik, Plate heat exchangers for process industry applications: enhanced thermal–hydraulic characteristics of chevron plates, in: R.M. Manglik, A.D. Kraus (Eds.), Process, Enhanced and Multiphase Heat Transfer, Begell House, New York, 1996, pp. 267–276.
[4] W.M. Kays, A.L. London, Compact Heat Exchangers, McGraw-Hill, New York, 1984.
[5] S.M. Flockhart, R.S. Dhariwal, Experimental and numerical investigation into the flow characteristics of channels etched in silicon, Journal of Fluids Engineering 120 (1998) 291–295.
[6] R.K. Shah, A.L. London, Laminar flow forced convection in ducts, supplement 1, in: Advances in Heat Transfer, Academic, New York, 1978.

[7] R.K. Shah, M.S. Bhatti, Laminar convective heat transfer in ducts, in: S. Kakaç, R.K. Shah, W. Aung (Eds.), Handbook of Single-Phase Convective Heat Transfer, Wiley, New York, 1987 (Chapter 3).
[8] A. Lawal, A.S. Mujumdar, Laminar flow and heat transfer in power-law fluids flowing in arbitrary cross-sectional ducts, Numerical Heat Transfer 8 (1985) 217–244.
[9] R.M. Manglik, A.E. Bergles, Numerical modeling and analysis of laminar flow heat transfer in non-circular compact channels, in: B. Sundén, M. Faghri (Eds.), Computer Simulations in Compact Heat Exchangers, Computational Mechanics Publications, Southampton, UK, 1998 (Chapter 2).
[10] R.M. Manglik, J. Ding, Laminar flow heat transfer to viscous power-law fluids in double-sine ducts, International Journal of Heat and Mass Transfer 40 (1997) 1379–1390.
[11] R.M. Manglik, A.E. Bergles, Fully developed laminar heat transfer in circular-segment ducts with uniform wall temperature, Numerical Heat Transfer Part A 26 (1994) 499–519.
[12] T.M. Harms, M.A. Jog, R.M. Manglik, Effect of temperature dependent viscosity variations and boundary conditions on fully developed laminar forced convection in a semicircular duct, Journal of Heat Transfer 120 (1998) 600–605.
[13] S.G. Etemad, A.S. Mujumdar, Effects of variable viscosity and viscous dissipation on laminar convection heat transfer of a power-law fluid in the entrance region of a semi-circular duct, International Journal of Heat and Mass Transfer 38 (1995) 2225–2238.
[14] R.M. Manglik, P. Fang, Effect of eccentricity and thermal boundary conditions on laminar fully developed flow in annular ducts, International Journal of Heat and Fluid Flow 16 (1995) 298–306.
[15] Y. Asako, M. Faghri, Three-dimensional laminar heat transfer and fluid flow characteristics in the entrance region of a rhombic duct, Journal of Heat Transfer 110 (1988) 855–861.
[16] Y. Asako, M. Nakamura, M. Faghri, Developing laminar flow and heat transfer in the entrance region of regular polygonal ducts, International Journal of Heat and Mass Transfer 31 (1988) 2590–2593.
[17] S.G. Etemad, Laminar heat transfer to viscous non-Newtonian fluids in non-circular ducts. PhD thesis, Department of Chemical Engineering, McGill University, Montreal, Canada, 1995.
[18] B. Sundén, M. Faghri, Computer Simulations in Compact Heat Exchangers, Computational Mechanics, Southampton, UK, 1998.
[19] R.K. Shah, Laminar flow friction and forced convection heat transfer in ducts of arbitrary geometry, International Journal of Heat and Mass Transfer 18 (1975) 849–862.
[20] B. Farhanieh, B. Sundén, Three-dimensional laminar flow and heat transfer in the entrance region of trapezoidal ducts, International Journal of Numerical Methods in Fluids 13 (1991) 537–556.
[21] Y. Asako, M. Faghri, B. Sundén, Three-dimensional laminar forced convection characteristics of wavy ducts with trapezoidal cross section for plate-fin heat exchanger, in: B. Sundén, M. Faghri (Eds.), Computer Simulations in Compact Heat Exchangers, Computational Mechanics Publications, Southampton, UK, 1998 Chapter 3.